Compact Fully Printed GPS/GNSS Antenna Using Embedded MTM-EBGs

Braden P. Smyth, *Member, IEEE*, Samuel Clark, *Graduate Student Member, IEEE*, Nikitha Kannan, *Student Member, IEEE*, and Ashwin K. Iyer, *Senior Member, IEEE*

***Abstract*— A compact and low-profile antenna for global navigation satellite systems (GNSSs), with particular optimization for triband Global Positioning System (GPS) coverage, is presented. A dual-band antenna is developed with the use of metamaterial-based electromagnetic bandgap structures (MTM-EBGs) that covers GPS L1, L2, and L5 bands and a majority of the GNSS spectrum. The patch antenna is fabricated on two sides of a single substrate sheet above a ground plane, with a 3-D printed polylactic acid (PLA) substrate spacer for simple fabrication. The antenna is fed by a wideband and planar feed network below the ground plane, and simulation and measurement results show good performance in terms of matching, gain, pattern shape, and axial ratio, demonstrating that this antenna is an excellent candidate for use with modern high-accuracy multiband and multisystem GPS/GNSS receivers.**

***Index Terms*— Circular polarization, feed network, global navigation satellite system (GNSS), Global Positioning System (GPS), metamaterial-based electromagnetic bandgap structure (MTM-EBG), metamaterials, microstrip patch antenna, multiband.**

I. Introduction

GLOBAL navigation satellite systems (GNSSs) are freely available and extensively used worldwide for position, navigation, and timing (PNT) services. Several GNSS satellite constellations have been deployed, including the United States' Global Positioning System (GPS), Europe's Galileo, Russia's GLONASS, and China's BeiDou (formerly COMPASS), along with several smaller regional navigation satellite systems (RNSSs) and satellite-based augmentation systems (SBASs). Reliance on these systems has increased dramatically in civilian, industrial, and military applications, and several billion devices worldwide now rely on precise PNT information [1], [2].

GNSS satellites broadcast right-hand circularly polarized (RHCP) signals within the frequency ranges of 1164–1300 MHz and 1559–1610 MHz, with specific bands varying for different systems. GPS, for example, uses three bands in this range, referred to as GPS L1 (1575.42 MHz), L2 (1227.60 MHz), and a recently introduced third band, L5 (1176.45 MHz); a bandwidth of ±12 MHz around each frequency is required for P(Y)- and M-code reception, although smaller bandwidths are acceptable for civilian use with C/A code. Operating a GPS receiver over several or all of these bands provides some distinct advantages. Multiple frequencies can be used to improve location accuracy by correcting errors such as those caused by propagation through the ionosphere, increase signal reliability particularly in the presence of multipath interference, enhance real time kinematic (RTK) positioning, improve PNT in difficult environments, such as urban canyons, and make the user less vulnerable to interference, jamming, and spoofing [3]. Using multiple GNSS constellations simultaneously enhances these advantages further [3], [4], and receivers with this capability are commercially available for extreme accuracy [1].

Reception of GNSS signals is highly dependent on the choice of antenna. Many antennas are large, bulky, and/or narrowband, suitable for only a part of the GNSS spectrum, for example, GPS L1 only. Low-precision systems may use small, single-band antennas with poor performance characteristics, boost gain with active antennas, or use assisted GPS (A-GPS) to improve detection speed [5], but these approaches do not offer high levels of accuracy or reliability. Ideally, antennas should have specific properties, such as a nearly hemispherical pattern, good axial ratio to receive RHCP, and good front-to-back ratio (FBR) to mitigate multipath interference, all of which are difficult to maintain over the bandwidth of the GNSS spectrum.

Planar antenna structures are preferred to reduce antenna cost, as they balance simple fabrication and low profile with good performance [6]. Planar structures tend to be narrowband, but many methods have been developed to overcome this issue. For example, some early multiband GPS antennas used stacked patch configurations, and while performance in each band is generally degraded, dual-band or triband operation can be achieved [7], [8], [9].

Many multiband planar antennas have been constructed specifically for GPS applications, typically prioritizing GPS L1 and L2 due to both the relatively recent introduction of L5, and the difficulty of covering all GPS/GNSS bands. Planar geometries are typically loaded for dual-band operation, and high permittivity dielectrics are used for miniaturization [9], [10], [11], [12], [13]. Planar printed structures have also been

Manuscript received 2 June 2024; revised 14 August 2024; accepted 27 August 2024. Date of publication 9 September 2024; date of current version 30 October 2024. This work was supported in part by Infinite Electronics Inc., in part by KP Performance Antennas, and in part by the Natural Sciences and Engineering Research Council (NSERC) of Canada. *(Corresponding author: Ashwin K. Iyer.)*

Braden P. Smyth, Samuel Clark, and Ashwin K. Iyer are with the Department of Electrical and Computer Engineering, University of Alberta, Edmonton, AB T6G 2R3, Canada (e-mail: iyer@ece.ualberta.ca).

Nikitha Kannan was with the Birla Institute of Technology and Science-Pilani, Pilani 333031, India. She is now with Nvidia, Santa Clara, CA 95051 USA.

Color versions of one or more figures in this article are available at https://doi.org/10.1109/TAP.2024.3452939.

Digital Object Identifier 10.1109/TAP.2024.3452939

© 2024 The Authors. This work is licensed under a Creative Commons Attribution-NonCommercial-NoDerivatives 4.0 License.
For more information, see https://creativecommons.org/licenses/by-nc-nd/4.0/

assembled in 3-D geometries for dual-band operation, although this increases the antenna profile [14], [15].

Planar antennas covering most or all of the GNSS spectrum have also been demonstrated in many works [16], [17], [18], [19], [20], [21], [22], [23], [24], [25], [26], [27], [28], [29], [30], [31]. These antennas are typically dual band, often designed for the upper band to cover GPS L1 and the broader lower band to cover GPS L2 and L5 due to their close proximity, incidentally or intentionally covering the full upper and lower GNSS L-bands as a result. In [18], shorting pins in a patch cause the excitation of two modes to cover the GNSS bands, while [19] loads the edge of the patch to increase bandwidth. A bowtie antenna above a high-impedance surface is designed in [20], and square-ring-shaped slots in a square patch are used in [24]. Stacked [26] or coupled [21] annular rings demonstrate good performance with an appropriate feed network, while rings are placed in the ground plane of a circular slotted antenna in [22]. An annular monopole with rectangular strips is used in [23]. Many planar antennas are additionally placed above a modified ground plane, such as a choke-ring structure or resistive sheet, to improve multipath mitigation, but at the expense of significant additional size, weight, and cost [29], [30], [31].

A challenge with these low-profile, wideband antennas is achieving an acceptable axial ratio at all frequencies for RHCP reception, since patch antennas are often linearly polarized or have circular polarization over only a small frequency range. A broad axial ratio bandwidth can be maintained, however, by feeding the antenna with four ports in sequential quadrature phase [27], [32], [33]. Planar circuits may be used to achieve this with configurations involving a network of circuit components (power dividers, phase shifters, and so on) as in [18], [21], [25], and [27], while other systems use lumped surface-mount components that are more compact, but also increase cost [19], [20]. The feed network is an important consideration in terms of antenna performance, losses, fabrication complexity, and physical antenna size.

A recent technology used to render antennas multiband is known as the metamaterial-based electromagnetic bandgap structure (MTM-EBG) [34]. The MTM-EBG structure may be embedded directly into patch antennas to increase functionality without taking up any additional space, with implementations that are fully printed and do not require vias, producing good radiating properties in all resonant bands [35], [36], [37]. This work explores the application of the MTM-EBG, in modified form [38], into a circular patch antenna for full GPS/GNSS coverage, fed by a wideband planar feed network for circular polarization across the spectrum.

Section II of this work begins with a brief investigation of single-band antennas covering parts of the GNSS spectrum to motivate subsequent design choices and introduces a novel MTM-EBG structure that is used to effectively combine the individual patches. The resulting dual-band antenna with a broad lower band, made possible with the choice of a cheap 3-D printed substrate, is presented in detail in Section III. A wideband feed network for the antenna is developed in Section IV, maintaining a planar design with simple pin feeds for easy construction. The feed and antenna are combined and fabricated in Section V, where measurements demonstrate good agreement with simulation results. While good performance is observed across most of the GNSS band, performance is rigorously characterized at GPS L1, L2, and L5 to demonstrate key performance metrics. Section VI concludes this work.

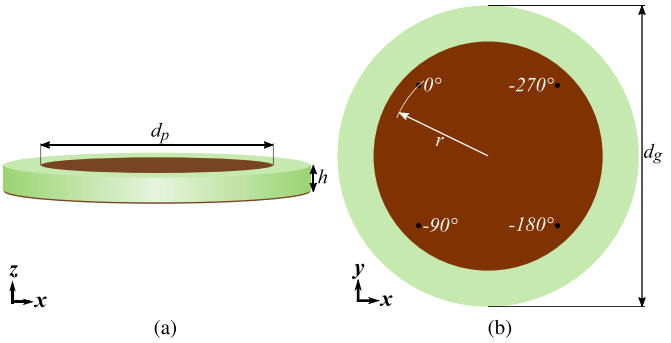

Fig. 1. (a) Side view of circular patch antenna. (b) Top view, with four pin feed locations and their relative phases indicated.

II. Theory

A. GPS/GNSS Antenna

The GPS/GNSS antenna in this work is constructed by effectively combining the geometry of single-band patch antennas that, respectively, cover the upper L-band (including GPS L1) and the lower L-band (including GPS L2 and L5) of the GNSS spectrum. The design of these conventional patches will briefly be investigated to establish important properties of the ultimate dual-band design.

Microstrip patch antennas typically have narrow bandwidths, and this is a challenge for multiband GPS/GNSS design; for example, for a conventional patch to cover both GPS L2 and L5 [each of which has a 24-MHz bandwidth for P(Y)-code reception], a minimum bandwidth of 6% is required when centered at the mean of these frequencies, 1202 MHz. Straightforward means of increasing patch antenna bandwidth include using low-permittivity dielectrics and increasing the substrate height [39]. A low-permittivity substrate with designable height that can be used for this application is polylactic acid (PLA), a standard inexpensive material used in 3-D printing, which has good dielectric properties at microwave frequencies [40]. The PLA used in this work was printed with an infill percentage of 100% and was measured using an open-ended coaxial probe to have a permittivity of $\epsilon_r = 2.64$; the loss tangent of this material is approximately $tan\delta = 0.0071$ [40].

Resulting conventional patch antenna designs with a PLA substrate are shown in Fig. 1. The diameters d_p of the L1 and L2/L5 antennas are 72.6 and 90.4 mm, respectively, and a ground plane diameter d_g of 120 mm was used. A substrate height h of 8.5 mm was chosen to provide sufficient impedance bandwidth to easily cover the GPS bands, as demonstrated by the simulated S-parameters shown in Fig. 2(a).

Circular polarization is achieved with the inclusion of four pins of equal angular spacing around the patch with successive quadrature phase. A common pin distance of $r = 32.0$ mm

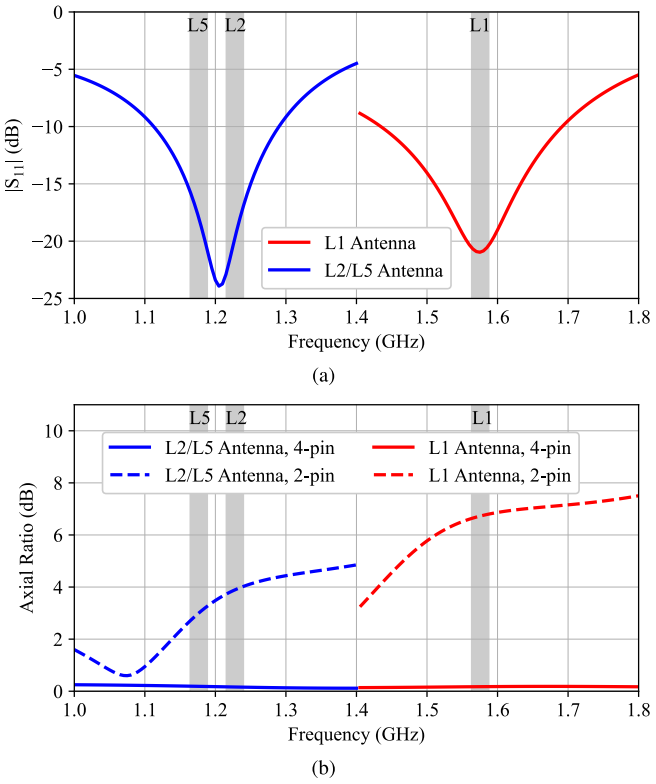

Fig. 2. (a) S-parameters of single-resonance antennas for operation over GPS L1 and L2/L5, with ±12-MHz bandwidths highlighted. (b) Broadside AR of single-band antennas with four versus two quadrature-phased pins.

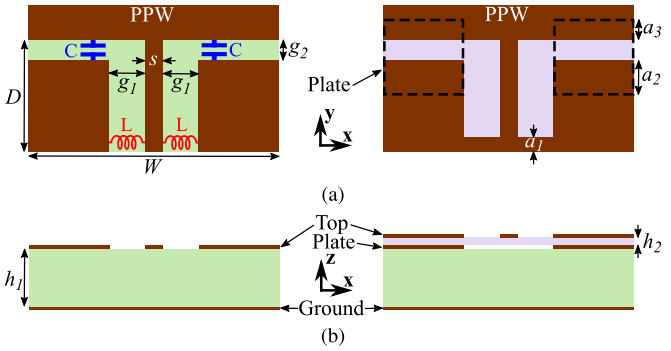

Fig. 3. (a) Top view and (b) cross-sectional view of MTM-EBG circuit model (left) and printed realization using strip inductors and parallel-plate capacitors (right). The printed version requires an additional dielectric layer. Both MTM-EBG unit cells are connected to a parallel-plate waveguide (PPW) structure that represents an antenna, and propagation is in the **y**-direction.

from the center of each patch enables good impedance matching. The broadside AR of this configuration is presented in Fig. 2(b) (solid lines), where it is notable that a very good RHCP polarization purity is observed over a large bandwidth, as expected. By comparison, keeping the same antenna design but only using two quadrature-fed pins to excite the antenna results in a dramatic increase in AR, also shown in Fig. 2(b) (dashed lines). Therefore, while the use of four appropriately phased feed locations requires a more complex feed structure, its substantially improved AR for the single-band antennas suggests it is a preferred method of excitation, as the extra pins enforce the appropriate phase conditions over the entire circumference of the antenna.

B. MTM-EBG Design

The L1 and L2/L5 antennas designed above differ only in patch radius d_p; all other parameters (d_g, h, and r) remain fixed. Therefore, to create a single patch antenna that operates in both bands, the patch radius must be made a function of frequency. An electrically small structure that provides a bandgap at L1 (such that d_p is shorter) and a passband with an appropriate phase response around L2/L5 (such that d_p is longer) is required. A structure that has proven to be ideally suited for such operation, especially for antenna applications [35], [36], is the MTM-EBG.

The MTM-EBG was first introduced as a means of suppressing parallel-plate noise in planar environments [34], but it has been applied to many microwave devices and antennas ever since to enable multiband operation without an increase in device size [35], [36], [41], [42]. It is especially useful for integration into planar structures of fixed electrical size, since it is electrically small, uniplanar, and has a predictable bandgap and phase response, due to analysis of its properties using multiconductor transmission line (MTL) theory [34].

Structurally, the MTM-EBG consists of a conductor-backed coplanar-waveguide-type (CBCPW) host MTL, periodically loaded with reactive elements, as shown in Fig. 3. The selection of its geometric properties and reactive loading allow its bandgap and phase properties to be designed, as dispersion properties of the MTM-EBG are calculated through Bloch analysis of a periodic set of unit cells. This has been demonstrated in a variety of previous works [35], [36], [41], [42], [43], and it is notable that even a single unit cell closely approximates the results of the Bloch analysis [35], [42], [43].

An MTM-EBG unit cell with carefully designed parameters can be embedded into a circular patch to make it dual band, thereby covering all three GPS bands, and a majority of the GNSS spectrum. To make the diameter of the patch frequency-dependent, an MTM-EBG unit cell with a bandgap at L1 is appended circumferentially around a patch of diameter $d_p = 72.6$ mm (which operates at L1), such that the nominal resonance of the patch at L1 is maintained. In order to resonate at L2/L5 as well, the MTM-EBG unit cell must effectively extend the patch diameter by 17.8 mm (to a total of 90.4 mm). Note that a large number of azimuthal unit cells can be added to the patch edge, such that each is approximately rectangular [34].

The cavity model of patch antennas predicts that the electrical length of the lowest-order excitation is approximately 180°; more exact expressions are available for circular patches [44], but this approximation works sufficiently well for the present application. The phase across the patch when resonating can then be expressed as follows:

$$180^\circ = \theta_0(f) + 2\theta_M(f) \tag{1}$$

where $\theta_0(f)$ is the phase of the 72.6-mm patch region and $\theta_M(f)$ is the phase across one MTM-EBG unit cell as a function of frequency (the factor of 2 arises, since the total diameter of the patch includes two MTM-EBG unit cells, one on either side). At L1, $\theta_0(L1) \approx 180^\circ$, so $\theta_M = 0^\circ$ (hence, the

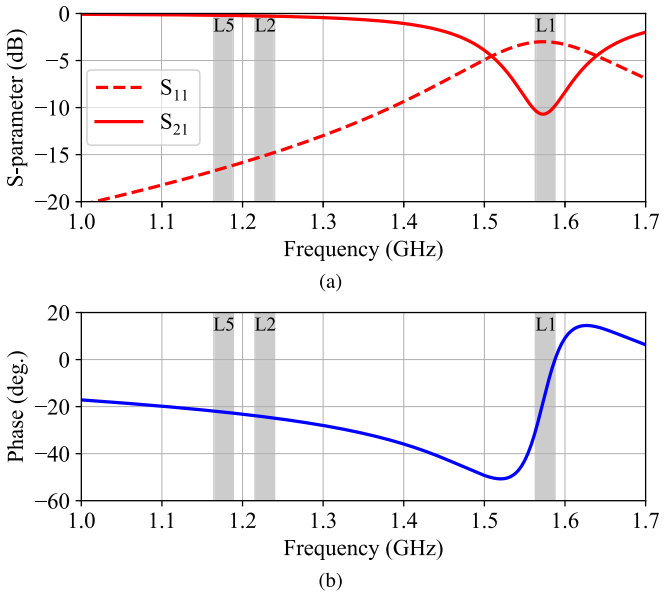

Fig. 4. (a) Magnitude (dB) of S-parameters for one MTM-EBG unit cell. (b) Phase of S_{21} for a single unit cell.

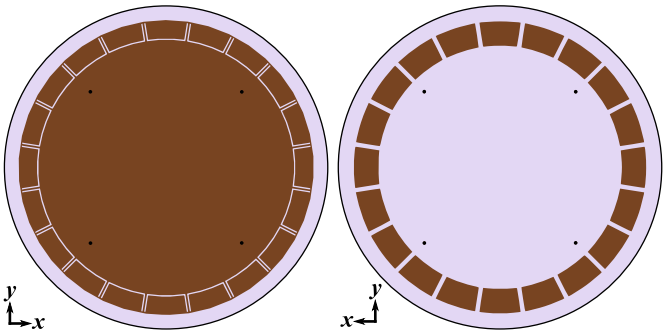

Fig. 5. (a) Top side and (b) bottom side of patch structure printed on 10-mil Rogers RO3006. The entire board sits atop an 8.5-mm-thick PLA layer and ground plane. Four quadrature-phased feed pin locations are indicated.

MTM-EBG bandgap), while at the lower resonant frequency of 1202 MHz, $\theta_0(L2/L5) = 138°$, so $\theta_M(L2/L5) = 21°$ for resonance.

An MTM-EBG unit cell is designed to have these properties using the aforementioned Bloch analysis. Dimensionally, and in reference to Fig. 3, the unit cell has geometric parameters of $D = 5.9$ mm, $W = 12.8$ mm, $s = 0.4$ mm, $g_1 = 0.5$ mm, and $g_2 = 0.5$ mm; the width was chosen so that exactly 20 unit cells are placed azimuthally along the patch edge. The unit cell is loaded with capacitors $C = 1.33$ pF and small inductors $L = 0.2$ nH. To verify the correct properties were obtained, a simulation of the unit cell embedded in a parallel-plate environment (to simulate the fields encountered in a patch antenna) was conducted. The bandgap and phase response of the unit cell are presented in Fig. 4. It is observed that a bandgap occurs at L1, while the required phase is produced near 1202 MHz.

Physical implementation of the unit cell can be achieved without the need for discrete chip capacitors and inductors by realizing them in printed form; compare the left- and right-hand sides of Fig. 3. The small inductances can simply be replaced by a small metallic strip, shown with width a_1 in Fig. 3(a). Capacitors have, in previous works, been realized with interdigitations; however, in the present case, the capacitance required is prohibitively large to use this method. Instead, parallel-plate capacitors with a capacitive gap height of h_2 can be used, as shown in Fig. 3(b), enabled by the addition of a thin substrate layer of thickness h_2. This novel implementation of the MTM-EBG is well suited for an application in an antenna where the main substrate is 3-D printed. Since the PLA substrate is not copper-plated, an additional substrate is required on which to print the patch itself; both sides of this substrate may be used to print the parallel-plate capacitors. The choice of the thin substrate material affects the parallel-plate capacitance of the MTM-EBG, but has a negligible effect on the antenna resonance frequency, which is mainly dependent on the PLA. A $h_2 = 0.254$-mm-thick Rogers 3006 substrate ($\epsilon_r = 6.15$, $\tan\delta = 0.002$, and clad in 1/2-oz copper) was chosen, and the required capacitances were achieved with the dimensions of $a_1 = 0.4$ mm, $a_2 = 5$ mm, and $a_3 = 1.7$ mm.

III. Triband GPS Antenna Design

The proposed MTM-EBG unit cell was implemented into a circular patch antenna for dual-band operation. The antenna consists of a ground plane, a PLA substrate, and the patch itself. The patch is printed on the thin Rogers RO3006 substrate with the capacitive plates of the MTM-EBG on the opposite side. Both sides of the patch substrate are shown in Fig. 5. The patch is fed by four copper pins that pass through circular apertures (radius of 2 mm) in a solid ground plane and proceed to pass through the PLA and RO3006 substrates to electrically connect to the patch itself. Four ports with excitations of equal magnitude and appropriate quadrature phase are assigned in simulation; realistic feeding of the patch will be considered in Section IV.

The antenna is tuned so that the inner patch diameter is 76.4 mm, while the overall diameter with the MTM-EBG unit cells is 88.2 mm, slightly smaller than the 90.4-mm diameter of the lower frequency patch. The only additional fabrication step compared with the conventional designs is a two-sided printing of the patch PCB, although no vias or more complicated geometries are required. The antenna remains low profile, and the cheap 3-D printed substrate ensures it is also low cost.

The dual-band antenna was simulated using Ansys HFSS, and the reflection coefficient is presented in Fig. 6(a). P(Y)-code reception bandwidths of ±12 MHz around all GPS frequency bands are highlighted, and good matching is observed in each band. The total 10-dB impedance matching bandwidths are 1126–1273 MHz and 1558–1599 MHz, which cover the majority of the GNSS spectrum, including Galileo E1, E5a, and E5b. The lower L-band could be shifted upward to provide full coverage of Galileo E6 as well, but optimization of the GPS bands with greater than 15 dB of matching was prioritized for the present design.

Gain patterns showing co-polarization (RHCP) and cross-polarization (LHCP) are provided for the antenna at each operating frequency in Fig. 6(b); only a single cut of the

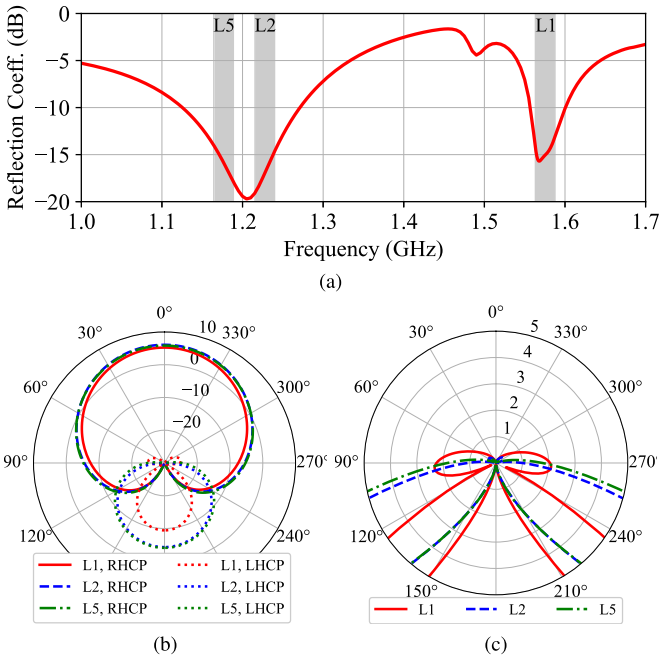

Fig. 6. (a) Simulated S_{nn} of GPS/GNSS antenna. n may be any of the four ports due to symmetry. (b) Simulated gain (dBic) and (c) AR (dB) at GPS operating frequencies.

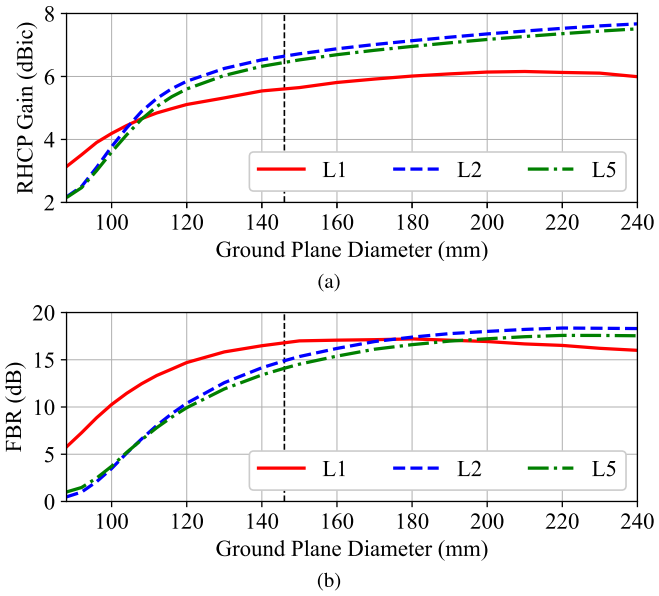

Fig. 7. (a) Broadside RHCP gain and (b) broadside FBR of antenna versus ground plane size. The vertical dashed line indicates ground plane diameter ultimately chosen to accommodate feed network.

pattern ($\phi = 0$) is shown due to azimuthal symmetry. For the ideal excitation of equal magnitude and quadrature phase at each port, excellent polarization purity is achieved, and RHCP gains of greater than 5 dBic are observed at broadside at all frequencies, with the radiation efficiencies of 54.7%/82.8%/83.7% and 3-dB beamwidths of 78°/86°/88° at L1/L2/L5, respectively. RHCP gain 10° above the horizon ranges from −5.3 to −3.3 dBic. AR is plotted in Fig. 6(c), and excellent performance is observed; polarization purity will, therefore, be dictated by performance of a realistic feed, as the antenna performs well in the ideal case.

Ground plane size will affect the radiation characteristics of the GPS antenna. For the presented results, a ground plane of $d_g = 146$ mm was used, but there may be cases in which a smaller ground plane (e.g., stand-alone miniaturized antenna) or a larger ground plane (e.g., antenna mounted on metallic body of vehicle or aircraft) is required. A study of some important radiation parameters versus ground plane size is, therefore, merited. Ground plane size versus broadside gain is presented in Fig. 7(a). Increasing the ground plane size results in increased broadside RHCP gain, as the beam is narrowed slightly; however, gain remains sufficiently high even as the ground plane shrinks, although the reduction in gain is attributed to increased LHCP radiated downward, and a degradation in multipath performance is expected as a result. This is characterized by FBR, defined as follows [3]:

$$FBR = \frac{G_{RHCP}(\theta)}{G_{LHCP}(180° - \theta)}. \tag{2}$$

It is observed in Fig. 7(b) that broadside FBR is low for small ground plane diameters, but rises above 15 dB in all bands as ground size increases.

IV. Feed Network

To feed the four-pin GPS antenna with a single input, a feed network that operates as a four-way power divider with sequential quadrature phase is required. A microstrip-based circuit was pursued.

In order for the feed network to provide the required phase and amplitude at all three GPS bands, the network must be either multiband or broadband (with about a 30% bandwidth). A broadband network was chosen, since many components are available with such bandwidths in the literature, and the feed network, which consists of many components, is less frequency-sensitive as a result. The microstrip-based feed network is designed over a solid ground plane, which may be used as a common ground with the antenna, while isolating each part from the other. The size of the antenna ground plane then depends partially on the size of the feed network. The GPS antenna will ultimately be fed by a single standard subminiature A (SMA) cable in an edge-launch configuration.

The designed feed network consists of three quadrature hybrid couplers (QHCs) and one differential phase shifter (DPS); a block diagram of these components, showing the output phase at each of the four ports, is given in Fig. 8(a). A broadband coupler was designed based on a multiloop circuit resembling a QHC with an extra branch [45], [46] and was miniaturized through meandering of some of the constituent transmission line segments. The DPS was based on [47]. Both components were designed on 50-mil Rogers 3006, which offered a good tradeoff between miniaturization of components and reasonable transmission line widths.

The QHCs and DPS were tuned individually before they were combined into the final layout that feeds the GPS antenna at the prescribed pin positions. This layout is shown in Fig. 8(b), with components that correspond to the block diagram indicated. The transmission line segments that lead to the pin locations are all of equal length to preserve the

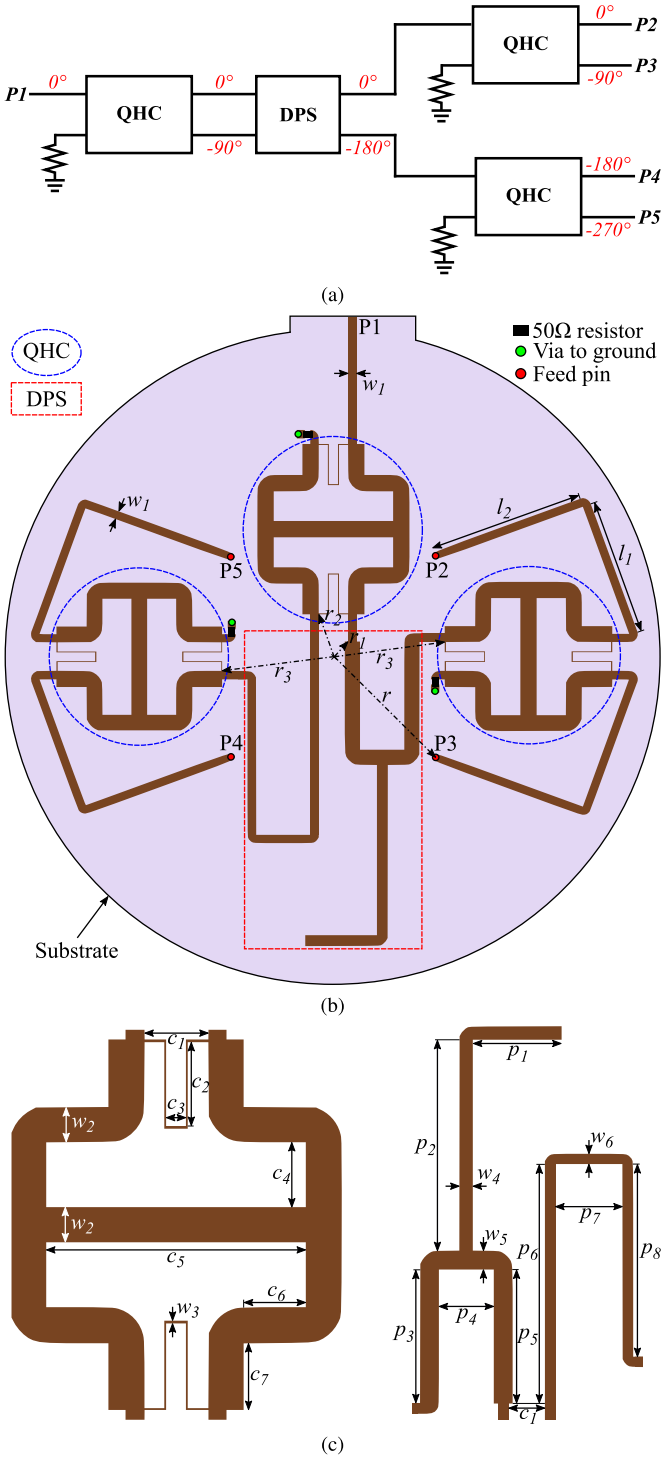

Fig. 8. (a) Proposed feed network consisting of three QHCs and a DPS, with signal phase at each node indicated. (b) Layout of feed network for GPS/GNSS antenna using broadband components. (c) QHC and DPS parameters, with dimensions given in Table I.

relative port phasing, and the overall substrate diameter is 146 mm. The input port extends to a flat edge protruding from the circular substrate to enable feeding with an SMA cable.

The QHC requires segments of high-impedance transmission lines with a width of 0.15 mm. This dimension may be reliably realized with some PCB-printing technologies, such as laser etching used in this work, and was, therefore, deemed acceptable. The QHC is also planar except for a 50-Ω resistor

TABLE I
FEED NETWORK DIMENSIONS WITH UNITS IN mm

$r = 32.00$	$r_1 = 4.64$	$r_2 = 9.64$	$r_3 = 25.00$
$l_1 = 30.58$	$l_2 = 34.77$	$w_1 = 1.78$	$w_2 = 3.50$
$w_3 = 0.15$	$w_4 = 2.31$	$w_5 = 3.30$	$w_6 = 1.78$
$c_1 = 6.57$	$c_2 = 8.67$	$c_3 = 2.04$	$c_4 = 6.66$
$c_5 = 26.40$	$c_6 = 6.41$	$c_7 = 6.81$	$p_1 = 15.84$
$p_2 = 37.70$	$p_3 = 23.98$	$p_4 = 9.87$	$p_5 = 23.98$
$p_6 = 42.77$	$p_7 = 12.15$	$p_8 = 34.41$	

TABLE II
FEED NETWORK PERFORMANCE

	Goal	L1	L2	L5
$\lvert S_{11}\rvert$ [dB]	<-15	-22.18	-15.66	-15.77
$\lvert S_{21}\rvert$ [dB]	-6.02	-6.31	-6.43	-6.77
$\lvert S_{31}\rvert$ [dB]	-6.02	-7.00	-6.95	-6.94
$\lvert S_{41}\rvert$ [dB]	-6.02	-6.50	-6.42	-6.45
$\lvert S_{51}\rvert$ [dB]	-6.02	-7.22	-6.93	-6.57
$\angle S_{31} - \angle S_{21}$ [deg.]	-90.0	-88.9	-88.1	-88.9
$\angle S_{41} - \angle S_{21}$ [deg.]	-180.0	-176.9	-174.7	-174.2
$\angle S_{51} - \angle S_{21}$ [deg.]	-270.0	-265.9	-262.8	-263.2

that is required to prevent reflections from the isolated port and a via to ground the resistor.

Performance in each GPS band is compared in Table II, which allows specific values of power division and relative phase to easily be compared. The first row of data shows that the feed is well matched, with return loss greater than 15 dB in all bands. Next, the feed network is designed for equal power division to each port, so the following four rows provide $|S_{n1}|$ in dB, where $n = (2, 3, 4, 5)$ are the four output ports; the maximum absolute difference in insertion loss at the four output ports is 0.5 dB at L2/L5 and 0.9 dB at L1. The remaining rows present phase shift referenced to port 2, which each successive port adding an additional phase lag of 90°. In all bands, port 3 is within 2°, port 4 is within 6°, and port 5 is within 8° of the ideal phase value. These deviations from the expected phase will degrade axial ratio to some extent, but the deviations are small enough that an acceptable AR was still anticipated.

Good broadband performance of the feed network suggests that it is a good candidate to feed the proposed antenna over the entire GNSS spectrum. Combination of the feed and antenna follows, with simulated and experimental results.

V. RESULTS

The antenna was fabricated in several steps. First, Board A (the patch/MTM-EBG layer; see Fig. 9) was fabricated on the required thin substrate with the use of an LPKF Protolaser U3 laser milling system for etching and LPKF ProtoMat S62 for routing and drilling holes in the pin locations. Board B (feed network/ground plane) was fabricated similarly with apertures through the ground plane through which the feed pins pass; metallic vias, resistors, and SMA connectors were added manually. Finally, the PLA substrate was 3-D printed to the appropriate size, leaving holes for the copper wire feed pins to pass through. The antenna was assembled with the soldering of four copper wire pins to the top of Board A and the bottom of Board B with the PLA layer in between,

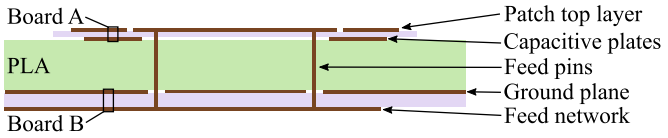

Fig. 9. Cross-sectional view of the GPS/GNSS antenna, showing two circuit boards for the patch and feed/ground, and the PLA substrate. Dimensions are not to scale.

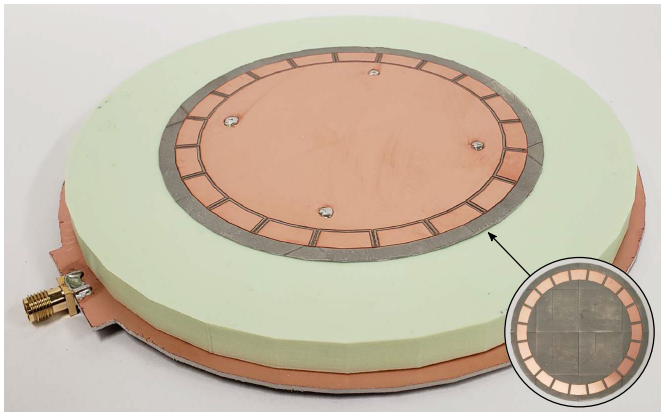

(a)

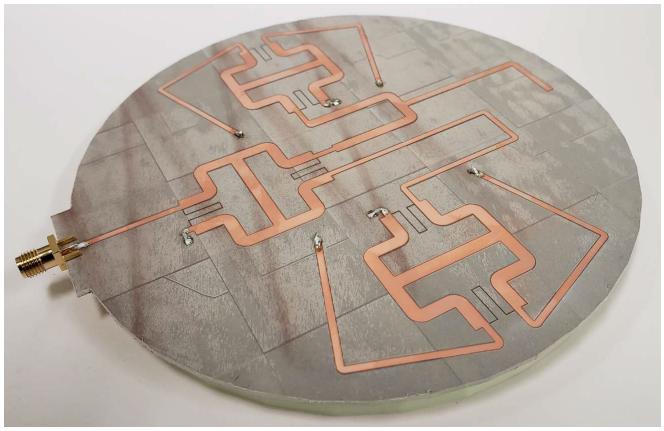

(b)

Fig. 10. Fabricated GPS/GNSS antenna. (a) Top view, with inset showing underside of patch. (b) Bottom view.

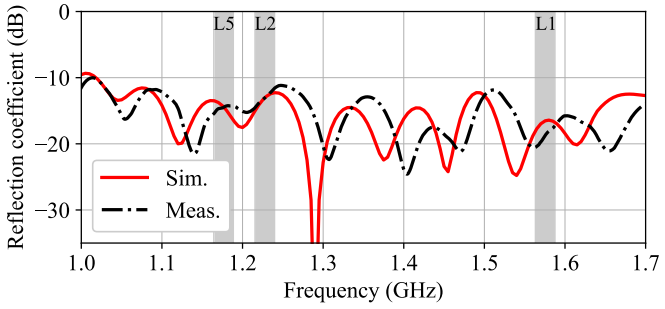

Fig. 11. Simulated and measured reflection coefficient of GPS/GNSS antenna with feed network.

completing the electrical connection and providing rigidity. An adhesive could be used for a stronger bond between layers. The fabricated antenna is shown in Fig. 10.

The GPS/GNSS antenna was measured both with a vector network analyzer (VNA) and in an anechoic chamber to fully characterize its properties. First, the reflection coefficient of the antenna with the feed network is presented in Fig. 11.

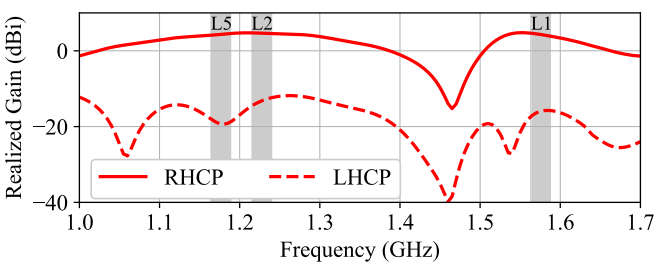

Fig. 12. Simulated broadside realized gain of antenna with feed network.

Matching greater than 10 dB is observed over the full GNSS range in simulation and measurement, although the clear dual-band operation is obscured by losses in the feed network at frequencies where the antenna is not matched; reflected power is dissipated in the QHC resistors. Realized gain can instead be used as a metric to determine the frequencies at which the antenna is radiating.

Broadside realized gain for the simulated antenna with feed network is plotted in Fig. 12, where good performance is again observed over the full GNSS spectrum, with the GPS bands, in particular, highlighted. Available facilities did not have the ability to accurately measure gain for comparison; however, normalized radiation patterns were measured in an anechoic chamber and are presented in Fig. 13. Results on the xz plane, which includes the SMA connector, are plotted in the left column and the yz plane on the right; good agreement in pattern shape, particularly for RHCP, is observed. The increase in LHCP is caused by the imperfect phase response of the feed network, and disagreements between simulation and measurement arise from the presence of cables and stands used to measure the antenna.

Despite increased cross-polarization, good AR is maintained in the upper hemisphere; simulated and measured results of AR patterns are provided in Fig. 14. Plots are shown in the yx plane so as not to include the SMA connector, but similar results are observed in either plane. Simulated AR is below 3 dB over the entire upper hemisphere, while measured 3-dB AR beamwidths of 162°/157°/138° are obtained above the horizon at L1/L2/L5, respectively.

Measured broadside FBR of the antenna is 13.0 dB at L1, 14.1 dB at L2, and 14.4 dB at L5, with simulation showing very good agreement with these results. As a function of angle, measured FBR is greater than 10 dB in all bands for nearly all of the upper hemisphere; the worst case is for L1, where FBR is greater than 10 dB for any $\theta < 82°$. It could be improved somewhat with a larger ground plane, as demonstrated in Fig. 7(b), or else choke rings, EBG, or other modified ground plane designs may be added to reduce the back lobe further [29], [48].

The proposed GPS antenna is compared with similar antennas in the literature in Table III. Low-profile antennas are included, particularly those employing a four-pin feed geometry, and some additionally use multipath mitigating ground planes, a technique which increases size, weight, and cost but most notably improves FBR. The proposed antenna is thinner than others reported and covers not just GPS frequencies but most of the GNSS spectrum. It performs

TABLE III
COMPARISON OF ANTENNA TO THE LITERATURE AT L1/L2/L5

	Size (mm^3)	Matching (dB)	Gain (dB)	FBR (dB)	AR (dB)	3-dB AR Beamwidth (deg.)
This Work	146×146×8.6	-17 / -13 / -14	5.5 / 6.6 / 6.8	13.0 / 14.4 / 14.4	1.7 / 2.2 / 1.1	162 / 157 / 138
[21]	200×200×21	$<$ -9.5 / $<$ -9.5 / $<$ -9.5	$>$ 5.2 / $>$ 5.2 / $>$ 5.2	Not Given	$<$ 2.1 / $<$ 2.1 / $<$ 2.1	$\sim$ 100 / $\sim$ 100 / $\sim$ 100
[20]	155×155×16	$<$ -10 / $<$ -10 / $<$ -8	4.95 / 6 / 5.7	$>$ 15 / $>$ 10 / $>$ 10	0.91 / 1.4 / 1.5	54 / 114 / 116
[13]	80×80×13	-14 / -14 / -	4.1 / 4.5 / -	$\sim$ 8 / $\sim$ 4 / -	2 / 3 / -	60 / 90 / -
[19]	136×136×10	$<$ -13 / $<$ -13 / -	6.8 / 6.4 / -	$\sim$ 13 / $\sim$ 16 / -	2.7 / 2.7 / -	Not Given
[27]	112×112×30	$<$ -10 / $<$ -10 / $<$ -10	4.8-7.33	$\sim$ 40 / $\sim$ 27 / $\sim$ 25	1.15-1.7	Not Given
[25]	124×129×15	$<$ -10 / $<$ -10 / $<$ -10	$\sim$ 5 / $\sim$ 5 / $\sim$ 5.6	$\sim$ 12 / $\sim$ 12 / $\sim$ 10	$<$ 2.5 / $<$ -2.5 / $<$ -1	Not Given
[28]*	160×160×40	$<$ -20 / $<$ -10 / $<$ -20	7.94 / 7.7 / 7.55	27 / 26 / 24	1.4 / 0.96 / 0.83	135 / 112 / 120
[29]*	254×254×126.5	$<$ -10 / $<$ -10 / -	$>$ 8 / $>$ 8 / -	$>$ 30 / $>$ 30 / -	$<$ 3 / $<$ 3 / -	115 / 143 / -
[30]*	167×167×69	$<$ -10 / $<$ -10 / $<$ -10	$>$ 6 / $>$ 7 / $>$ 6	$\sim$ 23 / $\sim$ 22 / $\sim$ 22	$<$ 2 / $<$ 3 / $<$ 3	Not Given
[31]*	160×160×85	$<$ -20 / $<$ -15 / $<$ -15	$\sim$ 5 / $\sim$ 4 / $\sim$ 4	$\sim$ 30 / $\sim$ 30 / $\sim$ 30	$\sim$ 1 / $\sim$ 1 / $\sim$ 1	Not Given

* Antenna design includes multi-path mitigating ground structure.

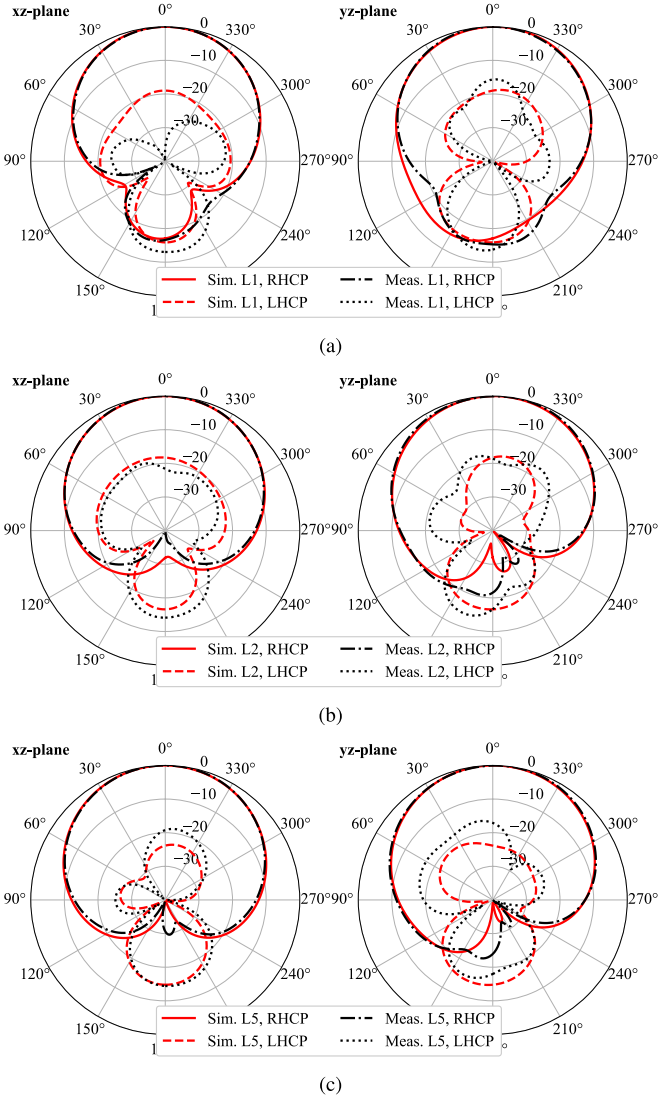

Fig. 13. Simulated and measured normalized radiation patterns of the GPS/GNSS antenna on the xz and yz planes for (a) L1, (b) L2, and (c) L5.

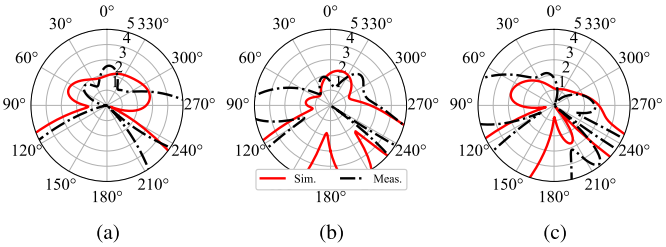

Fig. 14. Simulated and measured AR for the radiation patterns of the GPS/GNSS antenna on the yz plane for (a) L1, (b) L2, and (c) L5.

comparably well or better than the other antennas in categories of impedance matching, gain, FBR, AR, and AR beamwidth and demonstrates excellent radiation properties over the full upper hemisphere. Importantly, it also has consistent properties over all three GPS bands, which is not always the case for multimode or broadband antennas. The antenna is additionally based on solid theoretical foundations of the MTM-EBG, which allows designers to change properties for specific GNSS implementation cases, and smaller chip-based feed networks would allow for a reduction of ground plane size or an improvement in AR if even more precisely phased power division is achieved.

VI. CONCLUSION

A compact and low-profile GPS/GNSS antenna is presented in this work, with excellent operation at GPS L1, L2, and L5 and good coverage of most of the GNSS spectrum. The antenna consists of a patch layer with embedded MTM-EBG unit cells for dual-band operation with a 3-D-printed PLA substrate that maintains a low profile. The patch antenna is fed by four ports, and a feed network designed to supply equal power division and quadrature phase to each respective port was created with broadband microstrip-based components. The resulting antenna is shown to have excellent performance across the spectrum, with gain, pattern shape, and AR/FBR suitable for high-accuracy multiband, multisystem GNSS operation. The antenna system is, furthermore, robust with a planar structure and is cheap and easy to manufacture. The GPS/GNSS antenna is particularly well suited to applications with high multipathing, for example, on vehicles or drones in difficult locations, such as urban or natural canyons, or for military applications where jamming and spoofing are an operational risk.

ACKNOWLEDGMENT

The authors would like to thank CMC Microsystems for providing simulation tools and Rogers Corporation for their generous donation of substrate materials. They would also like to thank Samuel Zhu for 3-D printing the antenna substrate and Dr. Jamal Nasir for his assistance in optimizing the feed network.

REFERENCES

[1] D. Egea-Roca et al., "GNSS user technology: State-of-the-art and future trends," *IEEE Access*, vol. 10, pp. 39939–39968, 2022.

[2] European Union Agency for the Space Programme. (2024). *EUSPA EO and GNSS: Market Report*. Accessed: May 23, 2024. [Online]. Available: https://www.euspa.europa.eu/sites/default/files/2024-03/euspa_market_report_2024.pdf

[3] B. R. Rao, *GPS/GNSS Antennas*. Norwood, MA, USA: Artech House, 2013.

[4] J. Bu, K. Yu, N. Qian, X. Zuo, and J. Chang, "Performance assessment of positioning based on multi-frequency multi-GNSS observations: Signal quality, PPP and baseline solution," *IEEE Access*, vol. 9, pp. 5845–5861, 2021.

[5] F. van Diggelen, *A-GPS: Assisted GPS, GNSS, and SBAS*. Norwood, MA, USA: Artech House, 2009.

[6] J. J. H. Wang, "Antennas for global navigation satellite system (GNSS)," *Proc. IEEE*, vol. 100, no. 7, pp. 2349–2355, Jul. 2012.

[7] D. M. Pozar and S. M. Duffy, "A dual-band circularly polarized aperture-coupled stacked microstrip antenna for global positioning satellite," *IEEE Trans. Antennas Propag.*, vol. 45, no. 11, pp. 1618–1625, Nov. 1997.

[8] Y. Zhou, C.-C. Chen, and J. L. Volakis, "Dual band proximity-fed stacked patch antenna for tri-band GPS applications," *IEEE Trans. Antennas Propag.*, vol. 55, no. 1, pp. 220–223, Jan. 2007.

[9] G. Byun, S. Kim, and H. Choo, "Design of a dual-band GPS antenna using a coupled feeding structure for high isolation in a small array," *Microw. Opt. Technol. Lett.*, vol. 56, no. 2, pp. 359–361, Feb. 2014.

[10] R. Azaro, F. De Natale, M. Donelli, E. Zeni, and A. Massa, "Synthesis of a prefractal dual-band monopolar antenna for GPS applications," *IEEE Antennas Wireless Propag. Lett.*, vol. 5, pp. 361–364, 2006.

[11] S. Gupta and G. Mumcu, "Dual-band miniature coupled double loop GPS antenna loaded with lumped capacitors and inductive pins," *IEEE Trans. Antennas Propag.*, vol. 61, no. 6, pp. 2904–2910, Jun. 2013.

[12] M. Chen and C. Chen, "A compact dual-band GPS antenna design," *IEEE Antennas Wireless Propag. Lett.*, vol. 12, pp. 245–248, 2013.

[13] C. Sun, H. Zheng, and Y. Liu, "Analysis and design of a low-cost dual-band compact circularly polarized antenna for GPS application," *IEEE Trans. Antennas Propag.*, vol. 64, no. 1, pp. 365–370, Jan. 2016.

[14] Y. Yang, J. Guo, B. Sun, and Y. Huang, "Dual-band slot helix antenna for global positioning satellite applications," *IEEE Trans. Antennas Propag.*, vol. 64, no. 12, pp. 5146–5152, Dec. 2016.

[15] H.-S. Tae, K.-S. Oh, W.-I. Son, W.-G. Lim, and J.-W. Yu, "Design of compact dual-band quadruple inverted-F/L antenna for GPS L1/L2 band," *IEEE Trans. Antennas Propag.*, vol. 61, no. 4, pp. 2276–2279, Apr. 2013.

[16] B. Rama Rao, M. A. Smolinski, C. C. Quach, and E. N. Rosario, "Triple-band GPS trap-loaded inverted L antenna array," *Microw. Opt. Technol. Lett.*, vol. 38, no. 1, pp. 35–37, Jul. 2003.

[17] A. E. Popugaev, R. Wansch, and S. F. Urquijo, "A novel high performance antenna for GNSS applications," in *Proc. 2nd Eur. Conf. Antennas Propag. (EuCAP)*, Edinburgh, U.K., Nov. 2007, pp. 1–5.

[18] C. Sun, Z. Wu, and B. Bai, "A novel compact wideband patch antenna for GNSS application," *IEEE Trans. Antennas Propag.*, vol. 65, no. 12, pp. 7334–7339, Dec. 2017.

[19] J. Wei, S. Liao, Q. Xue, and W. Che, "Highly integrated multifunctional antenna for global navigation satellite system," *IEEE Trans. Antennas Propag.*, vol. 70, no. 12, pp. 12305–12310, Dec. 2022.

[20] B. Babakhani, S. K. Sharma, and G. Mishra, "Wideband circularly polarized his backed fan-shaped antenna with directional patterns covering L1-L5 GPS bands," *Microw. Opt. Technol. Lett.*, vol. 59, no. 3, pp. 497–500, Mar. 2017.

[21] Y.-Q. Zhang, X. Li, L. Yang, and S.-X. Gong, "Dual-band circularly polarized annular-ring microstrip antenna for GNSS applications," *IEEE Antennas Wireless Propag. Lett.*, vol. 12, pp. 615–618, 2013.

[22] S. Mishra, S. Das, S. S. Pattnaik, S. Kumar, and B. K. Kanaujia, "Low-profile circularly polarized planar antenna for GPS L1, L2, and L5 bands," *Microw. Opt. Technol. Lett.*, vol. 62, no. 2, pp. 806–815, Feb. 2020.

[23] N. Agrawal, A. K. Gautam, and R. Mishra, "Design of low volume circularly polarized annular ring-shaped planar antenna for GPS applications," *Int. J. RF Microw. Comput.-Aided Eng.*, vol. 31, no. 7, Jul. 2021, Art. no. e22698.

[24] X. Qing and Z. N. Chen, "A compact circularly polarized slotted patch antenna for GNSS applications," *IEEE Trans. Antennas Propag.*, vol. 62, no. 12, pp. 6506–6509, Dec. 2014.

[25] Q. Liu, Y. Li, Z. Mo, and Y. Liu, "Compact broadband circularly-polarised directional universal GNSS antenna with symmetric radiation pattern and stable near-zenith coverage," *IET Microw., Antennas Propag.*, vol. 11, no. 5, pp. 657–663, Apr. 2017.

[26] J. Li, H. Shi, H. Li, and A. Zhang, "Quad-band probe-fed stacked annular patch antenna for GNSS applications," *IEEE Antennas Wireless Propag. Lett.*, vol. 13, pp. 372–375, 2014.

[27] F. Tamjid, F. Foroughian, C. M. Thomas, A. Ghahreamani, R. Kazemi, and A. E. Fathy, "Toward high-performance wideband GNSS antennas-design tradeoffs and development of wideband feed network structure," *IEEE Trans. Antennas Propag.*, vol. 68, no. 8, pp. 5796–5806, Aug. 2020.

[28] S. X. Ta, H. Choo, I. Park, and R. W. Ziolkowski, "Multi-band, wide-beam, circularly polarized, crossed, asymmetrically barbed dipole antennas for GPS applications," *IEEE Trans. Antennas Propag.*, vol. 61, no. 11, pp. 5771–5775, Nov. 2013.

[29] M. Sun et al., "Compact hybrid choke rings for dual-band circularly polarized GPS antenna," *IEEE Antennas Wireless Propag. Lett.*, vol. 22, pp. 9–13, 2023.

[30] W. EnCheng, W. Zhuopeng, and C. Zhang, "A wideband antenna for global navigation satellite system with reduced multipath effect," *IEEE Antennas Wireless Propag. Lett.*, vol. 12, pp. 124–127, 2013.

[31] L. Du and Y. Fu, "A small wideband low-multipath GNSS antenna using resistive film," *IEEE Antennas Wireless Propag. Lett.*, vol. 12, pp. 1045–1048, 2013.

[32] F. Bilotti and C. Vegni, "Design of high-performing microstrip receiving GPS antennas with multiple feeds," *IEEE Antennas Wireless Propag. Lett.*, vol. 9, pp. 248–251, 2010.

[33] M. Qu, L. Deng, M. Li, L. Yao, and S. Li, "Compact sequential feeding network with quadruple output ports and its application for wideband circularly polarized antenna," *IEEE Access*, vol. 6, pp. 31891–31898, 2018.

[34] S. Barth and A. K. Iyer, "A miniaturized uniplanar metamaterial-based EBG for parallel-plate mode suppression," *IEEE Trans. Microw. Theory Techn.*, vol. 64, no. 4, pp. 1176–1185, Apr. 2016.

[35] B. P. Smyth, S. Barth, and A. K. Iyer, "Dual-band microstrip patch antenna using integrated uniplanar metamaterial-based EBGs," *IEEE Trans. Antennas Propag.*, vol. 64, no. 12, pp. 5046–5053, Dec. 2016.

[36] B. P. Smyth and A. K. Iyer, "Low-profile uniplanar dual-band and dual-polarized microstrip patch antenna using embedded MTM-EBGs," *IEEE Trans. Antennas Propag.*, vol. 69, no. 7, pp. 3645–3653, Jul. 2021.

[37] B. P. Smyth, S. Barth, and A. K. Iyer, "A low-profile tri-band microstrip GPS circular patch antenna with integrated MTM-EBGs," in *Proc. Int. Conf. Electromagn. Adv. Appl. (ICEAA)*, Honolulu, HI, USA, Aug. 2021, p. 115.

[38] B. P. Smyth, N. Kannan, S. Clark, and A. K. Iyer, "Compact multi-band GPS antenna using MTM-EBGs," presented at the Int. Symp. Electromagn. Theory, Vancouver, BC, Canada, May 2023.

[39] D. M. Pozar, "Microstrip antennas," *Proc. IEEE*, vol. 80, no. 1, pp. 79–91, Jan. 1992.

[40] R. Colella, F. P. Chietera, and L. Catarinucci, "Analysis of FDM and DLP 3D-printing technologies to prototype electromagnetic devices for RFID applications," *Sensors*, vol. 21, no. 3, p. 897, Jan. 2021.

[41] S. Barth, B. P. Smyth, J. A. Brown, and A. K. Iyer, "Theory and design of dual-band microstrip networks using embedded metamaterial-based electromagnetic bandgap structures," *IEEE Trans. Antennas Propag.*, vol. 68, no. 3, pp. 1761–1772, Mar. 2020.

[42] B. P. Smyth and A. K. Iyer, "Multiband impedance matching using microstrip-embedded MTM-EBGs," *IEEE Trans. Microw. Theory Techn.*, vol. 71, no. 8, pp. 3404–3413, Aug. 2023.

[43] J. A. Brown, S. Barth, B. P. Smyth, and A. K. Iyer, "Compact mechanically tunable microstrip bandstop filter with constant absolute bandwidth using an embedded metamaterial-based EBG," *IEEE Trans. Microw. Theory Techn.*, vol. 68, no. 10, pp. 4369–4380, Oct. 2020.

[44] C. A. Balanis, *Antenna Theory: Analysis and Design*. Hoboken, NJ, USA: Wiley, 2005.

[45] S. Kumar, C. Tannous, and T. Danshin, "A multisection broadband impedance transforming branch-line hybrid," *IEEE Trans. Microw. Theory Techn.*, vol. 43, no. 11, pp. 2517–2523, Nov. 1995.

[46] D. A. Letavin and N. S. Knyazev, "Broadband miniature quadrature coupler on planar cells," in *Proc. 33rd Gen. Assem. Scientific Symp. Int. Union Radio Sci.*, Rome, Italy, Aug. 2020, pp. 1–4.

[47] S. Y. Zheng, W. S. Chan, and K. F. Man, "Broadband phase shifter using loaded transmission line," *IEEE Microw. Wireless Compon. Lett.*, vol. 20, no. 9, pp. 498–500, Sep. 2010.

[48] M. Maqsood, S. Gao, T. W. C. Brown, M. Unwin, R. de vos Van Steenwijk, and J. D. Xu, "A compact multipath mitigating ground plane for multiband GNSS antennas," *IEEE Trans. Antennas Propag.*, vol. 61, no. 5, pp. 2775–2782, May 2013.

Braden P. Smyth (Member, IEEE) received the B.Sc. degree in engineering physics and the Ph.D. degree in electrical engineering from the University of Alberta, Edmonton, AB, Canada, in 2016 and 2023, respectively.

He worked on the development of multifunctional antennas and microwave components using planar metamaterial-based electromagnetic bandgap structures. He is currently a Post-Doctoral Fellow with the Microwave, Millimetre-Wave, and MetaDevices (M3) Laboratory, University of Alberta. His current research interests include fundamental electromagnetic and antenna theory, metamaterial applications in microwave circuits, and antenna applications in RFID, GNSS/GPS, and millimeter-wave systems.

Dr. Smyth has been a member of the IEEE Antennas and Propagation Society since 2015. He received the two NSERC Undergraduate Student Research Awards during his B.Sc., the Alberta Innovates Graduate Student Scholarship, Doctoral Recruitment Scholarship, the IEEE APS Pre-Doctoral Research Grant in 2017, for research into metamaterial-based structures and antennas, and the IEEE Antennas and Propagation Society Fellowship in 2022. He has been an Officer of the IEEE Northern Canada Section since 2020.

Samuel Clark (Graduate Student Member, IEEE) received the B.Sc. (Distinction) degree in electrical engineering from the University of Alberta, Edmonton, AB, Canada, in 2020, where he is currently pursuing the Ph.D. degree in electrical engineering with the Microwave, Millimetre-Wave, and MetaDevices (M3) Laboratory.

He is a Laboratory Manager and a Laboratory Safety Associate with the Microwave, Millimetre-Wave, and MetaDevices (M3) Laboratory, University of Alberta. His research interests include periodic structure theory and applications, multiconductor transmission line theory, metamaterial applications in microwave circuits, and fundamental electromagnetic and antenna theory.

Mr. Clark has been a member of the IEEE Antennas and Propagation Society since 2021. He received the two NSERC Undergraduate Student Research Awards during his B.Sc. and the NSERC Canada Graduate Scholarship (Master's Level) in 2021.

Nikitha Kannan (Student Member, IEEE) received the B.E. degree in electronics engineering and the M.Sc. degree in physics from the Birla Institute of Technology and Science (BITS)-Pilani, Pilani, Rajasthan, India, in 2024.

During her academic program, she gained research experience through internships at prestigious institutions. In 2021, she interned with CSIR-National Aerospace Laboratories, Bengaluru, India. In 2022, she worked with the University of Alberta, Edmonton, AB, Canada, where she investigated antenna design using metamaterial-based electronic bandgap structures. In 2023, she pursued her thesis with Stony Brook University, Stony Brook, NY, USA. She is currently working with Nvidia, Santa Clara, CA, USA. Her research interests include fundamental electromagnetic and antenna theory, GNSS/GPS, and metamaterial applications in microwave circuits.

Ms. Kannan has been a member of IEEE since 2020. She received the CB Das Memorial Award for the top graduating student during her M.Sc. and the MITACS Globalink Research Internship Award.

Ashwin K. Iyer (Senior Member, IEEE) received the B.A.Sc. (Hons.), M.A.Sc., and Ph.D. degrees in electrical engineering from the University of Toronto, Toronto, ON, Canada, in 2001, 2003, and 2009, respectively, where he was involved in the discovery and development of the negative-refractive-index transmission-line approach to metamaterial design and the realization of metamaterial lenses for free-space microwave subdiffraction imaging.

He is currently a Professor with the Department of Electrical and Computer Engineering, University of Alberta, Edmonton, AB, Canada, where he serves as the Director of the Microwave, Millimetre-Wave, and MetaDevices (M3) Laboratory. He has co-authored a number of highly cited articles and four book chapters on the subject of metamaterials. His research interests include novel RF/microwave circuits and techniques, fundamental electromagnetic theory, antennas, sensors, and engineered metamaterials and metasurfaces, with an emphasis on their applications to microwave and optical devices, defense technologies, and biomedicine.

Dr. Iyer is a member of several IEEE AP-S Committees including its Administrative Committee. He was a recipient of the IEEE AP-S R. W. P. King Award in 2008, the IEEE AP-S Donald G. Dudley Jr. Undergraduate Teaching Award in 2015, the University of Alberta Provost's Award for Early Achievement of Excellence in Undergraduate Teaching in 2014, and the University of Alberta Rutherford Award for Excellence in Undergraduate Teaching in 2018. His students are the recipients of several major national and international awards for their research. He served/will serve as a Technical Program Committee Co-Chair for the 2025, 2020, 2016, and 2015 APS/URSI International Symposia. He serves as the Chair for the IEEE Northern Canada Section's Award-Winning Joint Chapter of the AP-S and MTT-S. From 2012 to 2018, he was an Associate Editor of IEEE TRANSACTIONS ON ANTENNAS AND PROPAGATION. He serves as a Track Editor. He was also a Guest Editor of IEEE TRANSACTIONS ON ANTENNAS AND PROPAGATION Special Issue on Recent Advances in Metamaterials and Metasurfaces. He is a Registered Member of the Association of Professional Engineers and Geoscientists of Alberta.